

Energetic Protons, Radionuclides and Magnetic Activity in Protostellar Disks

N. J. Turner

*Jet Propulsion Laboratory, California Institute of Technology, Pasadena, California 91109;
neal.turner@jpl.nasa.gov*

and

J. F. Drake

*Department of Physics, Institute for Physical Science and Technology, University of
Maryland, College Park, Maryland 20742*

ABSTRACT

We calculate the location of the magnetically-inactive dead zone in the minimum-mass protosolar disk, under ionization scenarios including stellar X-rays, long- or short-lived radionuclide decay, and energetic protons arriving from the general interstellar medium, from a nearby supernova explosion, from the disk corona, or from the corona of the young star. The disk contains a dead zone in all scenarios except those with small dust grains removed and a fraction of the short-lived radionuclides remaining in the gas. All the cases without exception have an “undead zone” where intermediate resistivities prevent magneto-rotational turbulence while allowing shear-generated large-scale magnetic fields. The mass column in the undead zone is typically greater than the column in the turbulent surface layers. The results support the idea that the dead and undead zones are robust consequences of cold, dusty gas with mass columns exceeding 1000 g cm^{-2} .

Subject headings: circumstellar matter — solar system: formation — stars: formation — instabilities — MHD

1. INTRODUCTION

Angular momentum transport is a key to the evolution of protostellar disks and the origins of the planets, as it governs the flow of raw materials toward the star (Bodenheimer

1995). Transport processes likely to be important include the turbulence resulting from the magneto-rotational instability (MRI; Balbus & Hawley 1991, 1998) and the stresses due to large-scale magnetic fields driving an outflow (Blandford & Payne 1982; Wardle & Königl 1993) or shearing within the disk (Turner & Sano 2008).

All of the magnetic angular momentum transport processes require the gas is sufficiently ionized to couple to the fields. Collisional ionization leads to good coupling only at the temperatures above 1000 K found very close to the star (Pneuman & Mitchell 1965; Umebayashi 1983; Nakano & Umebayashi 1988). In the overwhelming majority of the disk volume, the main ionization processes are non-thermal. Among the important non-thermal processes are the X-rays emitted by the young star (Glassgold et al. 1997), the cosmic rays arriving from interstellar space (Umebayashi 1983; Umebayashi & Nakano 1988), and the decay of radionuclides within the gas (Umebayashi & Nakano 1981). The basic difficulties in reaching high enough levels of ionization through these non-thermal processes are the large column of absorbing material and the high rate of recombination on the surfaces of dust particles. The X-rays and cosmic rays generally penetrate and ionize only the surface layers of the disk, leaving a region near the midplane where magnetic activity is suppressed (Gammie 1996; Sano et al. 2000; Ilgner & Nelson 2006a).

The absorption of X-rays and cosmic rays in the atmosphere means that the disk can be divided into three zones. In the upper layers, and in outer annuli where the mass column is low enough for the ionizing radiation to reach the midplane, the magnetic fields couple thoroughly to the gas, and magnetic forces drive turbulence through the MRI. In a “dead zone” near the midplane, the fields decouple from the gas, and magnetic forces are largely irrelevant. At resistivities between these extremes, magnetic fields decouple over scales comparable to the disk thickness, shutting off the MRI, but remain coupled over the disk radius. The radial gradient in orbital frequency can then shear out any weak radial magnetic field to generate toroidal fields, enabling angular momentum transport to continue (Turner & Sano 2008). The turbulent surface layers are thus separated from the midplane dead zone by an “undead zone” that becomes magnetically active when supplied with radial fields.

In this paper we explore whether three less well-studied additional sources of ionization can reduce the sizes of the dead and undead zones or make protostellar disks magnetically active throughout. The three ionization sources are high-energy particles from (1) a nearby supernova explosion (Fatuzzo et al. 2006), (2) the corona of the protostellar disk itself, and (3) the young star. We estimate the ionization rates to order of magnitude (§2) and calculate the resulting resistivities (§3) in the minimum-mass model of the protosolar disk (§4), finding the undead and dead zones shown in §5. A summary and conclusions are in §6.

2. IONIZATION

The base ionization rate in our calculations is set by the X-rays emitted from the vicinity of the young star (§2.1). Some of the models include also the decay of radioactive isotopes within the disk (§2.2). Our purpose is to explore the additional effects of energetic protons from three sources: the interstellar medium (§2.3), the disk corona (§2.4), and the stellar corona (§2.5). With the aim of determining whether the dead zone can be removed under favorable circumstances, we generally err on the high side in estimating the proton fluxes. The rates of ionization from the five processes are compared in §2.6.

2.1. Stellar X-Rays

The X-ray ionization is included because almost all lightly-obscured young solar-mass stars in the Orion nebula show X-ray emission (Garmire et al. 2000; Preibisch et al. 2005). The measured spread in luminosity is several decades, with a median around 2×10^{30} erg s⁻¹. Evidence that the X-rays strike the disks comes from the iron K α fluorescent emission detected in some pre-main-sequence stars having near-infrared excesses (Imanishi et al. 2001; Favata et al. 2005a; Tsujimoto et al. 2005; Giardino et al. 2007). Gas at distance r directly facing the star is ionized at a rate $\zeta_X = \sigma F_X / E_i \approx 5 \times 10^{-11}$ s⁻¹ (r/AU)⁻², using a flux F_X corresponding to the median X-ray luminosity, an energy requirement per ionization $E_i = 37$ eV, and an absorption cross-section $\sigma = 4.16 \times 10^{-24}$ cm² at photon energy 5 keV and Solar composition (Glassgold et al. 1997). Most of the disk however is ionized at much lower rates, because the photons enter at grazing angles and only the most energetic and least numerous reach the deep interior. Detailed Monte Carlo radiative transfer results for a 5 keV thermal source spectrum (Igea & Glassgold 1999), fitted assuming an inverse square falloff with the radius, yield an ionization rate

$$\zeta_X = 2.6 \times 10^{-15} \text{ s}^{-1} (r/\text{AU})^{-2} [\exp(-\Sigma_a/\Sigma_X) + \exp(-\Sigma_b/\Sigma_X)] \quad (1)$$

at columns greater than 1 g cm⁻², where $\Sigma_X = 8.0$ g cm⁻² is the X-ray absorption depth and Σ_a and Σ_b are the mass columns lying vertically above and below the point of interest.

2.2. Radionuclides

The decay of long-lived radionuclides, primarily ⁴⁰K (half-life 1.25 Gyr), gives an ionization rate $\zeta_{LR} = 6.9 \times 10^{-23}$ s⁻¹ at protosolar elemental abundances (Umebayashi & Nakano 1981). Short-lived radionuclides, primarily ²⁶Al (half-life 0.717 Myr), yield an ionization rate

$\zeta_{SR} = 3.7 \times 10^{-19} \text{ s}^{-1}$ (Stepinski 1992). The results of our calculations change little if we use instead the rates advocated by Umebayashi & Nakano (2009), which differ from these by between 9% and 55%. The radionuclide ionization rates will be substantially lower if the dust particles containing most of the heavy elements are absent. In some cases without grains we include no radionuclide ionization, while in others the rate is reduced 10 000-fold from the dusty calculations to account for the possibility that a small amount of the radioactive element occurs in the gas phase.

2.3. Interstellar Cosmic Rays

The first of three energetic proton sources we consider is the interstellar cosmic rays. Particles with energies above 0.1 GeV provide most of the ionizing effect at high mass columns (Umebayashi & Nakano 1981). Shielding by the contemporary Solar wind reduces the flux of interstellar cosmic rays reaching the top of the Earth’s atmosphere in the energy range up to a few GeV (Spitzer & Tomasko 1968). Estimates of the cosmic ray energy spectrum outside the heliosphere, reviewed by Indriolo et al. (2009), scatter around the levels inferred by Comstock et al. (1972) that we use here. The intensity $0.94(E_0 + E)^{-2.6} \text{ cm}^{-2} \text{ s}^{-1} \text{ sr}^{-1} \text{ GeV}^{-1}$ falls off with energy E above the proton rest energy $E_0 = 0.938 \text{ GeV}$. The particles with $E > 0.1 \text{ GeV}$ deliver an energy flux of approximately $0.01 \text{ erg cm}^{-2} \text{ s}^{-1}$, producing an ionization rate

$$\zeta_{CR} = 5 \times 10^{-18} \text{ s}^{-1} \left\{ \exp\left(\frac{-\Sigma_a}{\Sigma_{CR}}\right) \left[1 + \left(\frac{\Sigma_a}{\Sigma_{CR}}\right)^{\frac{3}{4}}\right]^{-\frac{4}{3}} + \exp\left(\frac{-\Sigma_b}{\Sigma_{CR}}\right) \left[1 + \left(\frac{\Sigma_b}{\Sigma_{CR}}\right)^{\frac{3}{4}}\right]^{-\frac{4}{3}} \right\} \quad (2)$$

under isotropic illumination of the disk surface (Umebayashi & Nakano 2009). The cosmic ray absorption depth $\Sigma_{CR} = 96 \text{ g cm}^{-2}$ (Umebayashi & Nakano 1981). Lacking good information about the degree to which the protosolar wind screened the inner protosolar disk from interstellar cosmic rays, and seeking a lower bound on the size of the undead and dead zones, we assume that the cosmic rays above 0.1 GeV reach the disk surface with the interstellar flux and energy spectrum.

A supernova explosion occurring within 10 pc of the young star could increase the cosmic ray energy density by about three orders of magnitude over the general interstellar value, based on the energetic-particle populations inferred from gamma-ray observations of supernova remnants (Fatuzzo et al. 2006). We therefore consider below the effects of a thousand-fold increase in the cosmic ray ionization rate.

2.4. Disk Corona

The second energetic proton source we consider is the atmosphere of the accretion disk itself. Forbidden optical line emission and central Balmer absorptions in the spectra of T Tauri stars indicate the presence of low-density overlying gas with temperatures in the range 5 000 to 10 000 K (Kwan 1997) similar to the Solar chromosphere. Models of the heating and cooling balance show that such temperatures can be produced by the stellar ultraviolet and X-ray irradiation (Kamp & Dullemond 2004; Glassgold et al. 2004; Nomura et al. 2007). Furthermore, many T Tauri disks produce winds with speeds of 10 to 100 km s⁻¹ (Hartigan et al. 1995; Takami et al. 2001; Pyo et al. 2002; Azevedo et al. 2007), typically surrounding a faster central jet. Since magnetic forces likely drive the winds, we assume below that the Alfvén speeds approach the escape speed in the extended atmospheres of the disks.

Under similar conditions in the Solar chromosphere and corona, fast magnetic reconnection and shocks lead to the acceleration of protons to high energies, as reviewed by Miller et al. (1997). Fast reconnection requires plasma in the Hall regime, so that the whistler or kinetic Alfvén driving waves are not dissipated (Cassak et al. 2005). The electron-ion collision frequency ν_{ei} must be less than the electron cyclotron frequency Ω_{ce} . In the atmosphere of the disk around a young Solar-mass star, the ratio of the two frequencies is

$$\frac{\nu_{ei}}{\Omega_{ce}} \approx 0.01 \left(\frac{n}{10^{10} \text{ cm}^{-3}} \right) \left(\frac{T}{10^4 \text{ K}} \right)^{-3/2} \left(\frac{r}{1 \text{ AU}} \right)^{1/2}, \quad (3)$$

using expressions from Mitchner & Kruger (1973) with the Coulomb logarithm set to 10. Fast reconnection can thus occur in the tenuous disk atmosphere. Reconnection in the dense, cold disk interior presumably is due to the slower Sweet-Parker mechanism.

Reconnection in the Solar corona produces a mix of thermal and non-thermal particles. The temperature of the thermal component is such that the downstream gas pressure is approximately equal to the upstream magnetic pressure. Similar conversion of magnetic energy to heat in the disk corona yields the virial temperature 10 eV $(r/\text{AU})^{-1}$. Reconnection can thus plausibly contribute to the heating and stirring indicated by the central Balmer absorptions (Kwan 1997) and by the Doppler-broadened emission line of ionized neon at 12.8 μm in TW Hydrae (Herczeg et al. 2007). The thermal particles do not affect the dead zone as they have little penetrating power.

The maximum energy of the non-thermal particles is approximately equal to the product of the particle charge q , the electric field strength, and the length over which the particles are accelerated. The electric field $|\mathbf{v} \times \mathbf{B}|/c$ is proportional to the reconnection speed $|\mathbf{v}|$, which we set equal to the Alfvén speed v_A . The lengths of magnetic loops in the disk corona

depend on the rate of reconnection relative to shear (Uzdensky & Goodman 2008). When shear dominates, loops may reach sizes comparable to the radius r , which we choose as the acceleration distance. The maximum energy of the particles produced during reconnection

$$E_{rec} = q \left(\frac{v_A B}{c} \right) r \approx 100 \text{ GeV} \left(\frac{n}{10^{10} \text{ cm}^{-3}} \right)^{1/2}, \quad (4)$$

so the high-energy tail extends into the regime of penetrating cosmic rays above 0.1 GeV.

The luminosity of the particles accelerated by reconnection in the disk corona is bounded above by the rate of gravitational energy release due to accretion. The accretion energy per unit area and unit time leaving each side of the disk around a young solar analog T Tauri star is about $3 \times 10^5 (\dot{M}/10^{-8} M_\odot \text{ yr}^{-1})(r/\text{AU})^{-3}$ times the energy flux in ordinary interstellar cosmic rays, where \dot{M} is the mass flow rate. Much of the accretion flux takes the form of thermal radiation from the disk photosphere, while some fraction is in magnetic fields that rise into the corona before dissipating. Results from shearing-box MHD calculations (Miller & Stone 2000) suggest the fraction is of order 10%. Some part of the coronal magnetic energy is converted through reconnection and shocks into the kinetic energy of non-thermal protons. We assume the proportion is similar to the contemporary Sun, where magnetic energy is dissipated at approximately $10^{27} \text{ erg s}^{-1}$, judging from the mean X-ray luminosity. The Sun and solar wind produce a flux at 1 AU of about one proton with energy exceeding 0.1 GeV, per square centimeter per second, comparable to the interstellar cosmic ray flux outside the heliosphere, according to data from the GOES satellite energetic particle sensors (Mewaldt et al. 2007) and to analyses of tracks produced in lunar rocks over the past few million years (Reedy & Marti 1991). The corresponding solar luminosity in particles above 0.1 GeV is around $10^{24} \text{ erg s}^{-1}$, or 0.1% of the rate of dissipation of magnetic energy. We thus infer that the overall fraction of the disk accretion energy that rises into the corona in the form of magnetic fields and is converted to energetic protons is 10^{-4} . Perhaps half the particles travel downward and strike the disk surface, yielding an ionisation rate ζ_{DP} that is $10(r/\text{AU})^{-3}$ times the demodulated interstellar cosmic ray value.

2.5. Stellar Corona

The third source of energetic protons we consider is the corona and inner wind of the young Sun. The contemporary Sun accelerates ions to cosmic ray energies. The reconnection of opposing magnetic fields with Alfvén speed v_A produces ions of mass m with energies of order mv_A^2 , according to observations near 1 AU in the Solar wind (Gosling et al. 2005) and to particle-in-cell models (Krauss-Varban & Welsch 2007; Drake et al. 2009a). Flaring regions in the Solar corona have densities of 10^9 to 10^{10} cm^{-3} (Benz et al. 1983; Krucker et al.

2008) and fields around 50 G, yielding protons with energies in the tens of keV range. How these seed particles reach much higher energies remains unclear. Ideas include repeated shock crossings (as reviewed by Malkov & Drury 2001) and magnetic reconnection (Lazarian & Opher 2009; Drake et al. 2009b).

The Sun produced more energetic particles when young: the X-ray flares observed in young stars, scaled by the solar relationship between X-ray luminosity and proton emission, indicate a 10^5 -fold enhancement in energetic protons compared to contemporary solar levels (Feigelson et al. 2002). Such an enhancement appears to be consistent with a spallation origin for ^{26}Al and other short-lived radionuclides whose decay products occur in primitive chondritic meteorites (Gounelle et al. 2006). In addition, the magnetic fields of young Solar-mass stars are strong enough for reconnection to produce large numbers of seed particles with energies above an MeV. T Tauri stars have kilogauss surface-averaged magnetic fields, three orders of magnitude stronger than the modern Sun (Johns-Krull et al. 1999; Johns-Krull 2007), while the densities of gas on coronal magnetic loops, inferred from the emitted X-rays, are around 10^{10} cm^{-3} (Favata et al. 2005b; Jardine et al. 2006). Absorption of the X-rays by foreground coronal material indicates columns also consistent with such densities (Robrade & Schmitt 2007). The characteristic energy of the seed protons produced in reconnection under these conditions is 10 MeV if the fields are uniformly-distributed, or larger if as is likely the fields are patchy across the face of the star.

Lacking better knowledge of the arrangement of the magnetic fields near the star, we cannot say whether the stellar coronal protons are channeled back into the star, out along open field lines into a wind, or toward the disk which may reach or penetrate the boundary of the stellar magnetosphere. Since our objective is a minimum size for the dead zone, we shall assume that the protons propagate in straight lines like the X-rays, reaching all parts of the disk surface unimpeded.

One must also bear in mind that most of the protons are produced in flares lasting only hours or days. The flare particles will reduce the size of the dead zone in the disk if the ionization created in one flare persists till the next. Calculations of the ionization due to X-ray flares suggest that the recombination time is less than the interval between flares unless the abundance of the dust in the disk is greatly reduced (Ilgner & Nelson 2006c). A more conservative estimate of the contribution of the stellar energetic particles comes from scaling the modern Sun up to the X-ray luminosity corresponding to ζ_X . The effective enhancement in the energetic protons is then only about 3.3 decades and the rate of ionization is comparable to that resulting from the stellar X-rays.

Nevertheless, in the interest of obtaining a minimum dead zone size, we treat the 10^5 -fold enhancement in the energetic protons as time-steady. The flux falls off roughly as the inverse

square of the distance, at distances much greater than the size of the stellar magnetosphere. Projection effects reduce the flux per unit disk area by about a factor ten, since the disk surface is inclined about 0.1 radian from the line of sight to the star. We take a surface ionisation rate ζ_{SP} of $10^4(r/\text{AU})^{-2}$ times the interstellar cosmic ray value. The particles from the coronae of the disk and star are assumed to decline with column in the same way as the interstellar cosmic rays, following eq. 2.

2.6. Ionization Processes Compared

The relative strengths of the different ionization processes are shown in figure 1 where the ionization rates at a column of 8 g cm^{-2} are plotted versus radius. Compared with the stellar X-rays, the stellar energetic protons are 40 times stronger and are the strongest process plotted. The disk coronal energetic protons are a few times weaker than the X-rays at 0.1 AU and fall off faster with distance. The interstellar cosmic rays are distance-independent and are stronger than the X-rays outside 16 AU. If enhanced a thousand times due to a nearby supernova, interstellar cosmic rays are stronger than the stellar X-rays outside 0.5 AU and are the strongest of all the processes outside 3 AU.

3. RESISTIVITY

Recombination in the gas phase and on grain surfaces balances the ionization processes in local chemical equilibrium. We find the balance by solving the reduced chemical reaction network discussed by Ilgner & Nelson (2006a). The ionization produces molecular ions which are destroyed through dissociative recombination, or by charge exchange with metal atoms which then recombine radiatively. Magnesium is chosen as a representative gas-phase metal because of its combination of high abundance and low desorption temperature. The amount initially in the gas is chosen to be 1% of the Solar magnesium abundance. Recombination also occurs on grains which can collide with electrons, ions and other grains. The grains are $1 \mu\text{m}$ in radius with an internal density 3 g cm^{-3} and a mass fraction 1% relative to the gas. In addition, molecules and atoms can become adsorbed on grain surfaces, reducing the gas phase abundances. The stiff set of ODEs representing the chemical kinetic equations is integrated to equilibrium using semi-implicit extrapolation (Press et al. 1992). The resulting electrical resistivity $\eta = 234\sqrt{T}/x_e \text{ cm}^2 \text{ s}^{-1}$ varies inversely with the electron fraction $x_e = n_e/n_n$, where n_e is the electron number density and n_n the total number density of neutrals (Blaes & Balbus 1994).

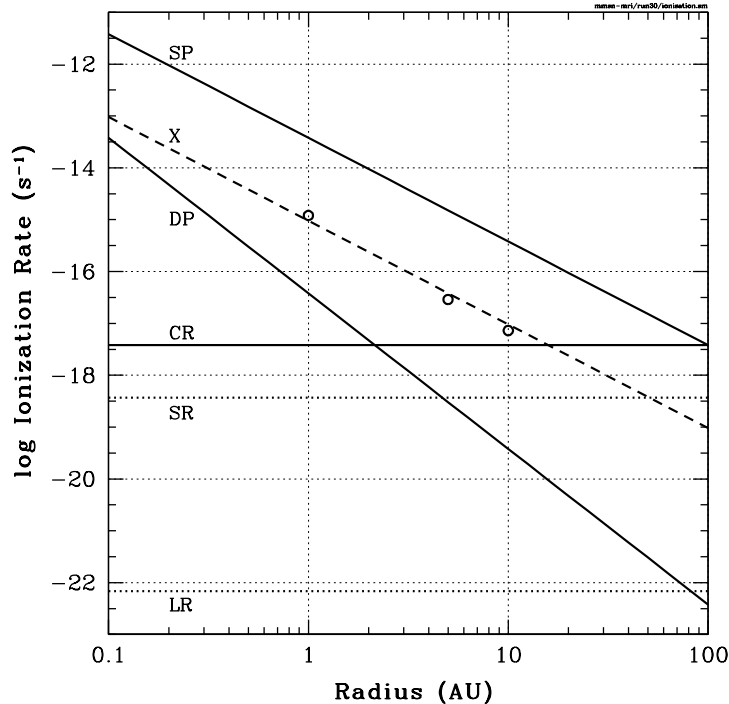


Fig. 1.— Ionization rates at column 8 g cm^{-2} versus the distance from the star. The dashed line shows the contribution of stellar X-rays, and the dotted lines the decay of short-lived (upper) and long-lived (lower) radionuclides. Among the three solid lines, the uppermost is for stellar energetic particles, the steepest shows the disk coronal particles, and the horizontal solid line is for interstellar cosmic rays. Large surface density is assumed and only radiation striking the top of the disk is included on this diagram. Circles indicate the results of the Monte Carlo X-ray transfer calculations by Igea & Glassgold (1999), scaled to a stellar X-ray luminosity $2 \times 10^{30} \text{ erg s}^{-1}$. The disk coronal particle estimate corresponds to a fraction 10^{-4} of the energy released by mass accretion at rate $10^{-8} M_{\odot} \text{ yr}^{-1}$.

4. DISK MODEL

We use the minimum-mass model of the protosolar disk (Hayashi et al. 1985), with surface mass density $\Sigma = 1700 \text{ g cm}^{-2} (r/\text{AU})^{-3/2}$ and temperature $T = 280 \text{ K} (r/\text{AU})^{-1/2}$ at distance r measured in astronomical units from a Solar-mass star. Vertical hydrostatic balance yields a volume density $\rho = (\Sigma/\sqrt{2\pi}H) \exp(-z^2/2H^2)$ declining with height z as a Gaussian, with a characteristic scale $H = c_s/\Omega$ that is the ratio of the isothermal sound speed c_s to the orbital frequency Ω .

5. DEAD ZONE

Magnetic stresses extract angular momentum from the disk only if the gas is sufficiently ionized to couple to the magnetic fields. Upper bounds on the allowed Ohmic resistivity η come from considering the dissipation scale. The minimum time for regenerating the field is the orbital period, while in the case of global magnetic fields, the characteristic size of the variations in the field is the distance to the star. The orbital shear acting on a weak radial seed field can produce large-scale toroidal fields faster than the fields diffuse away if

$$\frac{v_K^2}{\eta\Omega} > 10 \quad (5)$$

where v_K is the Keplerian orbital speed, Ω the orbital frequency and power-law radial variation is assumed for the magnetic fields (Turner & Sano 2008). Using a similar approach, MRI turbulence regenerates tangled magnetic fields if the resistivity is unable to erase magnetic variations over the MRI fastest-growing vertical wavelength $2\pi v_{Az}/\Omega$, where v_{Az} is the vertical component of the Alfvén speed. The criterion for MRI turbulence

$$\frac{v_{Az}^2}{\eta\Omega} > 1 \quad (6)$$

depends on the volume-averaged squared vertical Alfvén speed, whether the background magnetic field is vertical, toroidal, or zero (Sano & Stone 2002). Of eqs. 5 and 6, the turbulence condition is the more restrictive since the MRI wavelength typically is much less than the radius. The two criteria divide the disk into three unequal zones. In the active zone both conditions hold and strong magnetic activity is expected. In the undead zone the shear condition eq. 5 holds and the turbulence condition eq. 6 does not. Magnetic fields can then be generated by shear but not by MRI turbulence. In the dead zone, neither condition is satisfied and the gas is almost completely decoupled from the magnetic fields.

We determine the spatial extent of the magnetic activity in the minimum-mass protostellar disk by finding the locations where eqs. 5 and 6 are marginally satisfied. The ionization-recombination reaction network is solved to determine the resistivity on a grid of 60×250 points spaced logarithmically in radius and linearly in z/H , from $r = 0.1$ AU to 100 AU and from $z = 0$ to $5H$. The Alfvén speed in eq. 6 is calculated assuming the vertical magnetic fields at each radius have a pressure 1000 times less than the midplane gas pressure. Similar pressure ratios are found in ideal-MHD stratified shearing-box calculations (Miller & Stone 2000).

We first compute the sizes of the undead and dead zones in a fiducial model disk including ionization by stellar X-rays and long-lived radionuclides, and recombination on grains. For this calculation only, the chemical network is solved on a finer grid of 1000×1000 points

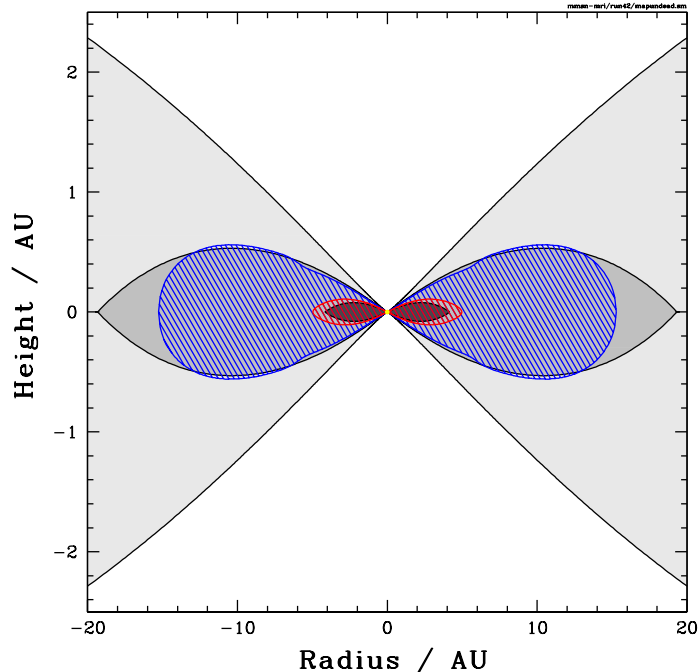


Fig. 2.— Dead zone (red) and undeath zone (blue) in the minimum-mass protosolar disk with well-mixed $1\text{-}\mu\text{m}$ dust grains at a mass fraction 1%. The ionization is due to stellar X-rays and long-lived radionuclides, and the vertical component of the magnetic field has pressure 0.1% of the midplane gas pressure. The vertical mass column exceeds 1, 10 and 100 g cm^{-2} in the light, medium and dark gray shaded regions, respectively. Note that the vertical scale is expanded by a factor four.

to more precisely determine the shape of the dead zone boundary. The results appear in figure 2. MRI turbulence reaches the midplane only outside 15 AU, while large-scale magnetic fields couple to the orbital shear at the midplane outside 5 AU. The boundary of the turbulent region approximately follows the contour of vertical column 10 g cm^{-2} , close to the X-ray absorption depth of 8 g cm^{-2} . Beyond 12 AU, turbulence occurs at greater columns because the lower densities mean slower recombination.

Results for eight different external ionization scenarios are shown in figure 3. All the scenarios include stellar X-ray ionization. The first has no other external sources of ionization, and corresponds to figure 2. The second includes ordinary interstellar cosmic rays. The third and fourth have the cosmic rays enhanced by factors 10^3 and 10^5 . The fifth and sixth instead have energetic particles from the disk corona, one with the scaling indicated in section 2.4 and the other with an ionization rate 100 times greater, corresponding to a

higher mass accretion rate of $10^{-6} M_{\odot} \text{ yr}^{-1}$. The seventh and eighth instead have protosolar energetic particles, one with the rate from section 2.5 and the other with a rate 100 times greater. All the calculations in figure 3 also include ionization by long-lived radionuclides, and recombination on grains.

The dependence on the radionuclide ionization rates and on the presence of grains is shown in the remaining figures. Short-lived radionuclides replace the long-lived radionuclides in figure 4. The dust is removed for figures 5 through 7, which include no radionuclides (figure 5), long-lived radionuclides with an abundance reduced by a factor 10^4 below the dusty cases (figure 6) and short-lived radionuclides with the same abundance reduction factor (figure 7).

The results with and without dust are quite different. With dust, the active zone fills the top 10 to 20 g cm^{-2} if the external ionization comes from stellar X-rays (figure 3). The active zone is little changed by ordinary cosmic rays or by energetic particles from the disk corona, since these are at most comparable to the X-rays near the bottom of the active zone. The active column increases to 20 to 100 g cm^{-2} if the cosmic ray flux is boosted a thousand times, and to 100 g cm^{-2} if the disk is exposed to the protosolar energetic particles inferred from X-ray flares in young stars. The column of material lying in the undead zone is three to ten times that in the active zone, while any remaining column is dead. Including short-lived radionuclides moves the dead zone boundary slightly deeper inside the disk while having little effect on the outer boundary of the undead zone (figure 4).

With no dust, the active layer fills the outermost 100 g cm^{-2} if the ionization is due to stellar X-rays, increasing to 100-200 g cm^{-2} if ordinary cosmic rays are added, and reaching 400-800 g cm^{-2} under an enhanced flux of cosmic rays, disk energetic particles, or protosolar energetic particles (figure 5). The undead column is two to ten times that in the active layer.

Including a small amount of radioactivity leaves the active layer unchanged because the radionuclide ionization rate is much less than that due to X-rays at the active layer boundary. The extra ionization can be important however in the regions shielded from the energetic protons and photons, yielding a bigger undead zone at the expense of the dead zone. The differences are slight with 0.01% of the long-lived radionuclides present in the gas (figure 6). By contrast, the whole dead zone becomes undead if 0.01% of the short-lived radionuclides is included (figure 7). Reducing the fraction to 0.001% leads to the appearance of a small dead zone just outside 0.1 AU. The threshold internal ionization rate for converting the entire dead zone into an undead zone is thus about $3 \times 10^{-5} \zeta_{SR} \approx 10^{-23} \text{ s}^{-1}$.

Cosmic rays from a nearby supernova can increase the active column by up to a factor eight over the interstellar cosmic ray case if the base of the active layer is defined solely by

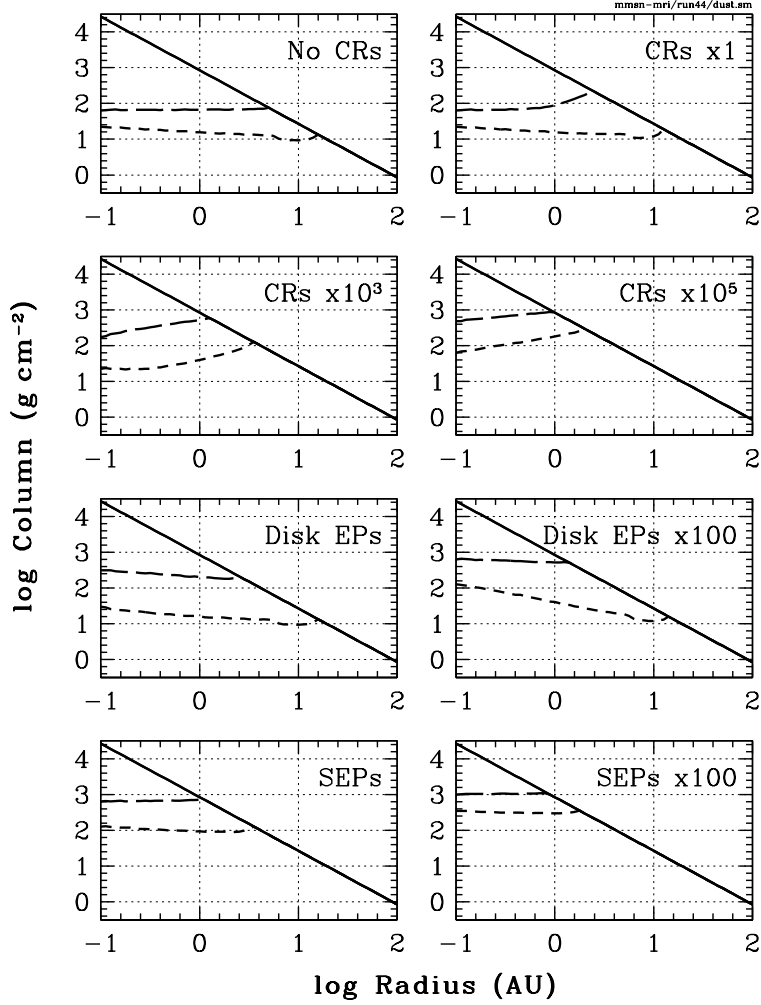


Fig. 3.— Column depth to the top of the undead zone (short dashes) and dead zone (long dashes) in the minimum-mass protosolar disk with well-mixed $1 \mu\text{m}$ dust grains at a mass fraction 1%. Solid lines show the midplane column. All eight ionization scenarios include stellar X-rays and long-lived radionuclides. The scenarios are (left to right and top to bottom): (1) no additional ionization, (2) with interstellar cosmic rays, (3) with cosmic ray flux enhanced 1000 times due to a nearby supernova, (4) with cosmic ray flux enhanced a further two orders of magnitude, (5) with energetic particles from the disk corona, (6) with the disk particles enhanced 100 times, (7) with energetic particles from the young Sun, and (8) with the protosolar particles enhanced 100 times.

the cosmic ray ionization rate (Fatuzzo et al. 2006). When the stellar X-rays and the rise in recombination rate with depth are included, the higher cosmic ray flux increases the active column at 1 AU only from 16 to 41 g cm^{-2} with dust (figure 3) and from 210 to 620 without

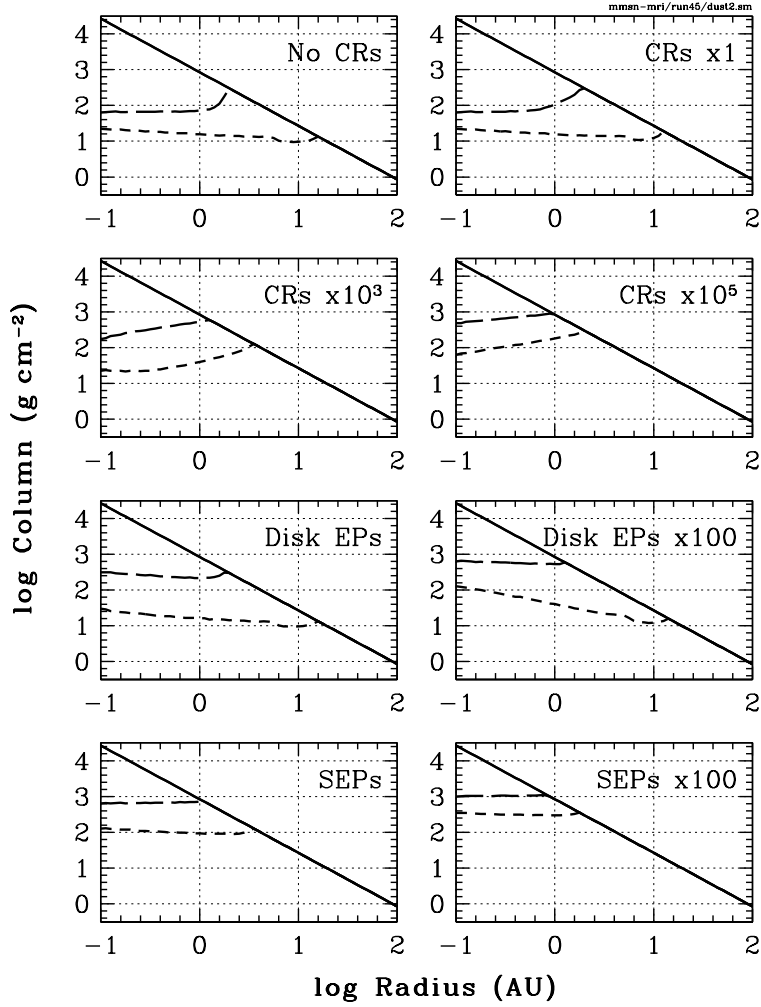


Fig. 4.— Column depth to the top of the undead zone (short dashes) and dead zone (long dashes) in the minimum-mass protosolar disk with dust grains and short-lived rather than long-lived radionuclides. The eight ionization scenarios are otherwise identical to figure 3.

(figure 5), factors of about three. The thousand-fold enhancement in the cosmic ray flux has less effect than removing the dust grains.

6. CONCLUSIONS

We calculated the locations of the undead and dead zones in the minimum-mass protosolar disk, under ionization scenarios including stellar X-rays, long- or short-lived radionuclide decay, and energetic protons arriving from the general interstellar medium, from a nearby

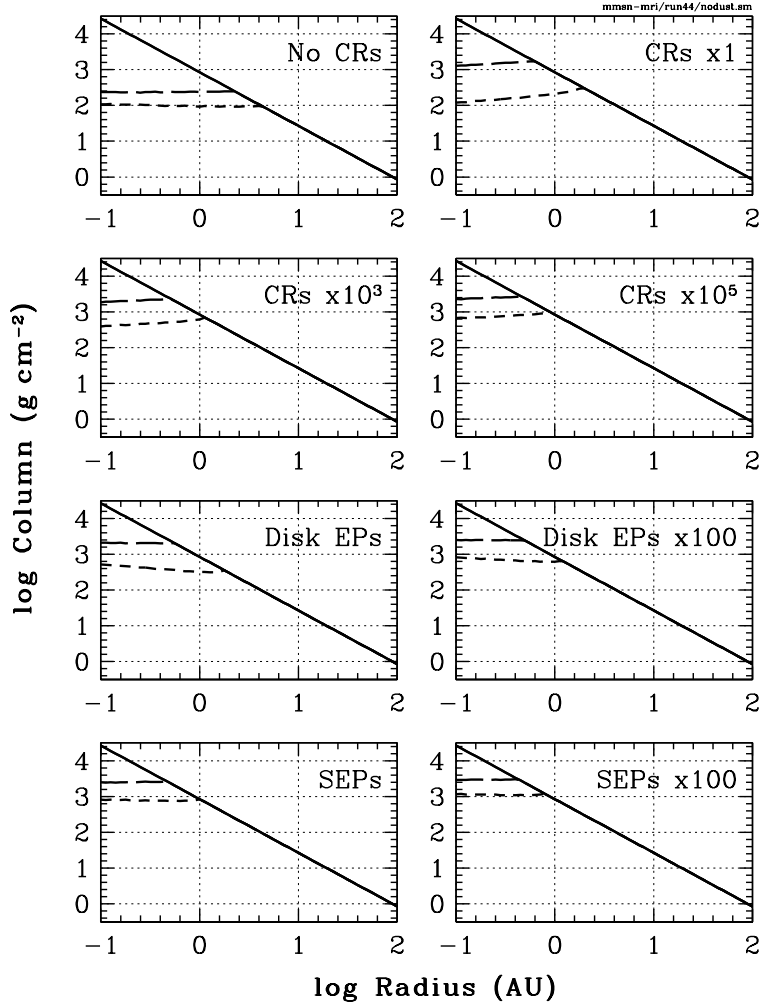


Fig. 5.— Column depth to the top of the undead zone (short dashes) and dead zone (long dashes) in the minimum-mass protosolar disk without dust. No radionuclide decay is included. The eight ionization scenarios are otherwise identical to figure 3.

supernova explosion, from the disk corona, or from the corona of the young star.

The disk contains an undead zone in all the scenarios. All have a dead zone except those with the dust removed and a small fraction of radioactive ^{26}Al remaining in the gas. Lacking short-lived radionuclides, even the strongest external ionization process considered, the stellar energetic particles, fails to eliminate the dead zone. The thickness of the magnetically coupled layers can increase over the local chemical equilibrium values we have computed, however, if ionized material mixes to the midplane before recombining. Slow recombination requires that dust is largely absent (Inutsuka & Sano 2005; Ilgner & Nelson 2006b; Turner et al. 2007; Ilgner & Nelson 2008).

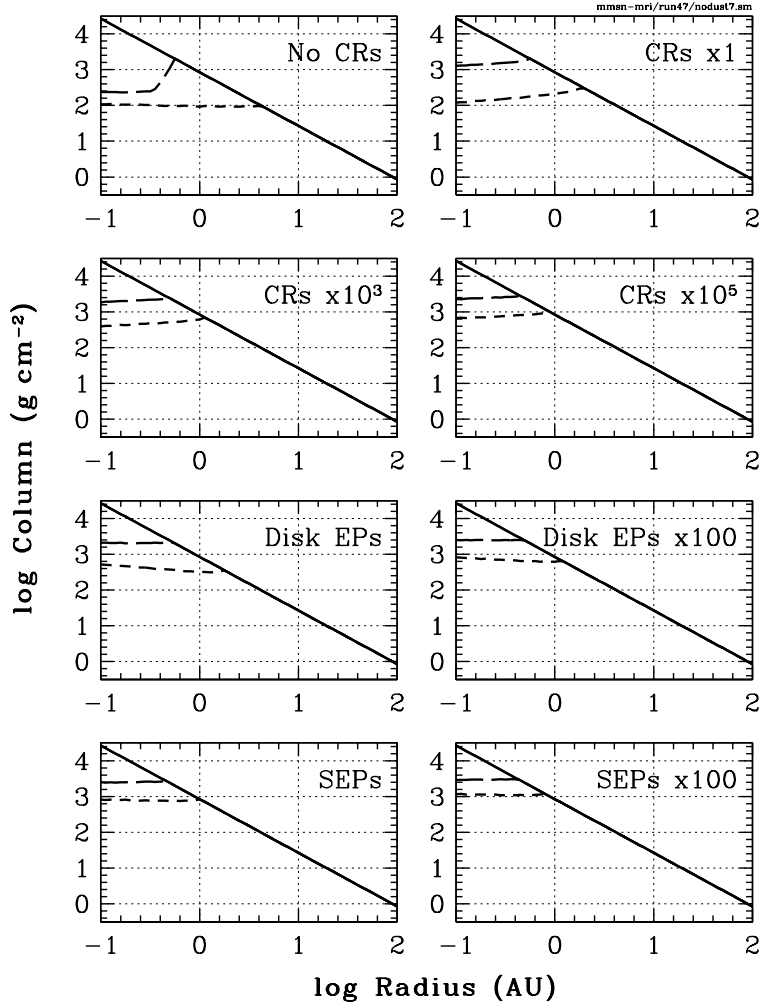


Fig. 6.— Column depth to the top of the undead zone (short dashes) and dead zone (long dashes) in the minimum-mass protosolar disk without dust, assuming that 0.01% of the long-lived radioactive ^{40}K remains in the gas phase. The eight ionization scenarios are otherwise identical to figure 3.

Placing these results in the context of existing work, we see that protostellar disks with no dead zone can be constructed by

1. Raising the temperature of the high-column material sufficiently for thermal ionization. The temperatures required are likely to be reached through either stellar illumination or accretion heating only within a few tenths of an AU of the star, at average mass flow rates. At the highest rates inferred for episodic accretion, thermal ionization of the interior may extend to a few AU. The central region could alternate between a cold

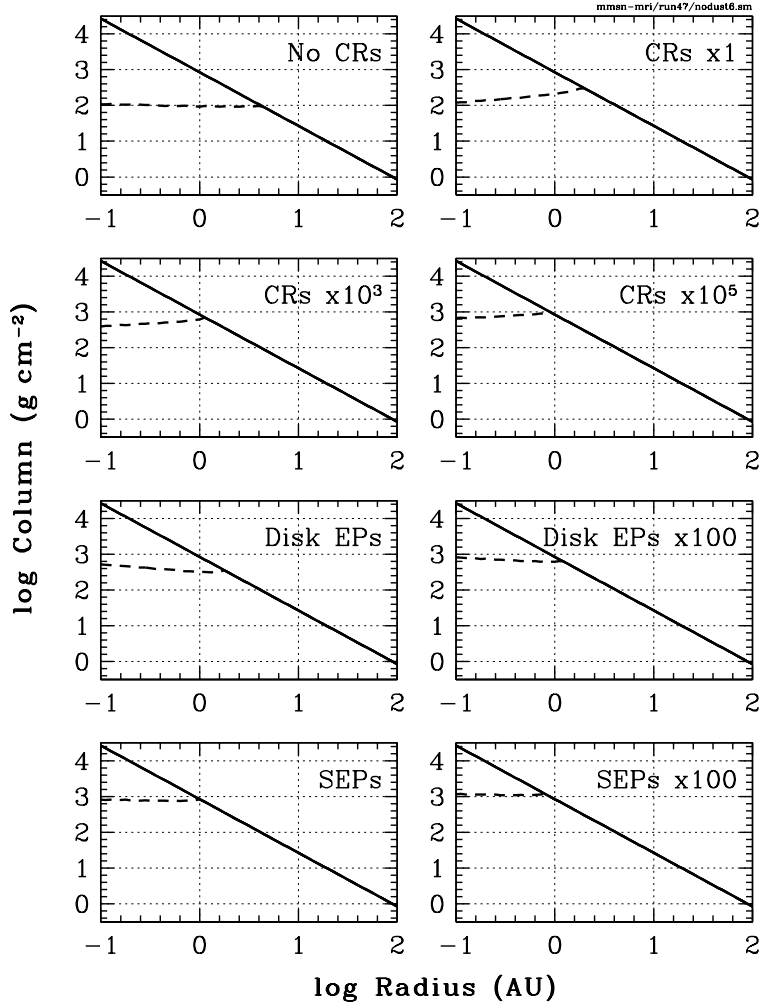


Fig. 7.— Column depth to the top of the dead zone (short dashes) in the minimum-mass protosolar disk without dust, assuming that 0.01% of the short-lived radioactive ^{26}Al is found in the gas phase. The eight ionization scenarios are otherwise identical to figure 3. The dead zone is eliminated under these conditions, but the dead zone remains.

state with a dead zone and a low accretion rate, and a hot, thermally-ionized state with a higher accretion rate (Armitage et al. 2001; Zhu et al. 2009).

2. Reducing the surface density below the minimum-mass protosolar model (Fromang et al. 2002). Forming planets under these conditions may be problematic. Lower surface densities could occur however during the dispersal of the disk, for example as X-ray ionized material is eroded from the inner edge (Chiang & Murray-Clay 2007).
3. Removing the small dust grains while retaining a fraction of the radionuclides in the

gas. The removal could occur through settling in the dead zone (Ciesla 2007) or incorporation into planetesimals. Making grains unimportant compared with gas-phase recombination requires reducing the dust abundance by several orders of magnitude (Sano et al. 2000), a difficult feat during planet formation, when solid bodies often collide fast enough to shatter and produce secondary particles (e.g. Wetherill & Stewart 1993).

Each of these three possibilities appears feasible only in limited circumstances. A fourth option involves ionization by the electrons carrying currents in the weakly-ionized disk interior (Inutsuka & Sano 2005). Further study of the microphysics of this process is desirable. We conclude that the dead and undead zones are robust consequences of cold, dusty gas without strong internal sources of ionization, having mass columns exceeding 1000 g cm^{-2} . Weaker turbulence at the midplane and reduced or fluctuating mass flows are likely under these conditions, and should be considered further in planet formation models.

We thank Eliot Quataert and the staff of the Theoretical Astrophysics Center at the University of California, Berkeley for their hospitality and comments, and Eric Feigelson, Hugh Hudson and Mark Wiedenbeck for useful discussions. The work was carried out in part at the Jet Propulsion Laboratory, California Institute of Technology, with support from the NASA Solar Systems Origins Program. Copyright 2009. All rights reserved.

REFERENCES

- Armitage P. J., Livio M. & Pringle J. E. 2001, MNRAS, 324, 705
- Azevedo, R., Folha, D. F. M., Gameiro, J. F., & Calvet, N. 2007, ApJ, 670, 1234
- Balbus, S. A., & Hawley, J. F. 1991, ApJ, 376, 214
- Balbus, S. A., & Hawley, J. F. 1998, Rev. Mod. Phys., 70, 1
- Benz, A. O., Barrow, C. H., Dennis, B. R., Pick, M., Raoult, A., & Simnett, G. 1983, Solar Physics, 83, 267
- Blaes, O. M., & Balbus, S. A. 1994, ApJ, 421, 163
- Blandford, R. D., & Payne, D. G. 1982, MNRAS, 199, 883
- Bodenheimer, P. 1995, ARA&A, 33, 199

- Cassak, P. A., Shay, M. A., & Drake, J. F. 2005, *Phys. Rev. Lett.*, 95, 235002
- Chiang, E., & Murray-Clay, R. 2007, *Nature Physics*, 3, 604
- Ciesla, F. 2007, *ApJ*, 654, L159
- Cisowski, S. M., & Hood, L. L. 1991, in “The Sun in Time”, ed. C. P. Sonett, M. S. Giampapa & M. S. Matthews (Tucson: Univ. of Arizona Press), 761
- Comstock, G. M., Hsieh, K. C., & Simpson, J. A. 1972, *ApJ*, 173, 691
- Drake, J. F., Swisdak, M., Phan, T. D., Cassak, P. A., Shay, M. A., Lepri, S. T., Lin, R. P., Quataert, E., & Zurbuchen, T. H. 2009, *J. Geophys. Res.*, 114, A05111
- Drake, J. F., Opher, M., & Swisdak, M. 2009, *ApJ*, submitted
- Fatuzzo, M., Adams, F. C., & Melia, F. 2006, *ApJ*, 653, L49
- Favata, F., Micela, G., Silva, B., Sciortino, S., & Tsujimoto, M. 2005, *A&A*, 433, 1047
- Favata, F., Flaccomio, E., Reale, F., Micela, G., Sciortino, S., Shang, H., Stassun, K. G., & Feigelson, E. D. 2005, *ApJS*, 160, 469
- Feigelson, E. D., Garmire, G. P., & Pravdo, S. H. 2002, *ApJ*, 572, 335
- Fromang, S., Terquem, C., & Balbus, S. A. 2002, *MNRAS*, 329, 18
- Gammie, C. F. 1996, *ApJ*, 457, 355
- Garmire, G., Feigelson, E. D., Broos, P., Hillenbrand, L. A., Pravdo, S. H., Townsley, L., & Tsuboi, Y. 2000, *AJ*, 120, 1426
- Giardino, G., Favata, F., Micela, G., Sciortino, S., & Winston, E. 2007, *A&A*, 463, 275
- Glassgold, A. E., Najita, J., & Igea, J. 1997, *ApJ*, 480, 344
- Glassgold, A. E., Najita, J., & Igea, J. 2004, *ApJ*, 615, 972
- Gosling, J. T., Skoug, R. M., McComas, D. J., & Smith, C. W. 2005, *J. Geophys. Res.*, 110, A01107
- Gounelle, M., Shu, F. H., Shang, H., Glassgold, A. E., Rehm, K. E., & Lee, T. 2006, *ApJ*, 640, 1163
- Hartigan, P., Edwards, S., & Ghandour, L. 1995, *ApJ*, 452, 736

- Hayashi, C., Nakazawa, K., & Nakagawa, Y. 1985, in: Black, D. C., & Matthews, M. S., Editors. *Protostars and Planets II* (Univ. of Arizona Press: Tucson), 1100
- Herczeg, G. J., Najita, J. R., Hillenbrand, L. A., & Pascucci, I. 2007, *ApJ*, 670, 509
- Igea, J., & Glassgold, A. E. 1999, *ApJ*, 518, 848
- Ilgner, M., & Nelson, R. P. 2006a, *A&A*, 445, 205
- Ilgner, M., & Nelson, R. P. 2006b, *A&A*, 445, 223
- Ilgner, M., & Nelson, R. P. 2006c, *A&A*, 445, 731
- Ilgner, M., & Nelson, R. P. 2008, *A&A*, 483, 815
- Imanishi, K., Koyama, K., & Tsuboi, Y. 2001, *ApJ*, 557, 747
- Indriolo, N., Fields, B. D., & McCall, B. J. 2009, *ApJ*, 694, 257
- Inutsuka, S., & Sano, T. 2005, *ApJ*, 628, L155
- Jardine, M., Collier Cameron, A., Donati, J.-F., Gregory, S. G., & Wood, K. 2006, *MNRAS*, 367, 917
- Johns-Krull, C. M., Valenti, J. A., & Koresko, C. 1999, *ApJ*, 516, 900
- Johns-Krull, C. M. 2007, *ApJ*, 664, 975
- Kamp, I., & Dullemond C. P. 2004, *ApJ*, 615, 991
- Krauss-Varban, D., & Welsch, B. T. 2007, in “Highlights of Astronomy”, vol. 14, ed. K. A. van der Hucht (IAU), p. 89
- Krucker, S., Saint-Hilaire, P., Christe, S., White, S. M., Chavier, A. D., Bale, S. D., & Lin, R. P. 2008, *ApJ*, 681, 644
- Kwan, J. 1997, *ApJ*, 489, 284
- Lazarian, A., & Opher, M. 2009, *ApJ*, submitted; arXiv:0905.1120
- Malkov, M. A., & Drury, L. O’C. 2001, *Rep. Prog. Phys.* 64, 429
- Mewaldt, R. A., Cohen, C. M. S., Mason, G. M., Haggerty, D. K., & Desai, M. I. 2007, *Space Sci Rev* 130, 323
- Miller, J. A., Cargill, P. J., Emslie, A. G., et al. 1997, *JGR*, 102, 14631

- Miller, K. A., & Stone, J. M. 2000, *ApJ*, 534, 398
- Mitchner, M., & Kruger, C. H. 1973, “Partially Ionized Gases” (New York: Wiley)
- Nakano, T., & Umebayashi, T. 1988, *Progr. Theor. Physics Suppl.*, 96, 73
- Nomura, H., Aikawa, Y., Tsujimoto, M., Nakagawa, Y., & Millar, T. J. 2007, *ApJ*, 661, 334
- Pneuman, G. W., & Mitchell, T. P. 1965, *Icarus*, 4, 494
- Preibisch, Th., Kim, Y.-C., Favata, F., et al. 2005, *ApJS*, 160, 401
- Press, W. H., Teukolsky, S. A., Vetterling, W. T., & Flannery, B. P. 1992, “Numerical Recipes in C”, 2nd ed (Cambridge: Cambridge University Press)
- Pyo, T.-S., Hayashi, M., Kobayashi, N., Terada, H., Goto, M., Yamashita, T., Tokunaga, A. T., & Itoh, Y. 2002, *ApJ*, 570, 724
- Reedy, R. C., & Marti, K. 1991, in “The Sun in Time”, ed. C. P. Sonett, M. S. Giampapa & M. S. Matthews (Tucson: Univ. of Arizona Press), 260
- Robrade, J., & Schmitt, J. H. M. M. 2007, *A&A*, 473, 229
- Sano, T., Miyama, S. M., Umebayashi, T., & Nakano, T. 2000, *ApJ*, 543, 486
- Sano, T., & Stone, J. M. 2002, *ApJ*, 577, 534
- Spitzer, L., & Tomasko, M. G. 1968, *ApJ*, 152, 971
- Stepinski, T. F. 1992, *Icarus*, 97, 130
- Takami, M., Bailey, J., Gledhill, T. M., Chrysostomou, A., & Hough, J. H. 2001, *MNRAS*, 323, 177
- Tsujimoto, M., Feigelson, E. D., Grosso, N., Micela, G., Tsuboi, Y., Favata, F., Shang, H., & Kastner, J. H. 2005, *ApJS*, 160, 503
- Turner, N. J., & Sano, T. 2008, *ApJ*, 679, L131
- Turner, N. J., Sano, T., & Dziourkevitch N. 2007, *ApJ*, 659, 729
- Umebayashi, T. 1983, *Progr. Theor. Phys.*, 69, 480
- Umebayashi, T. & Nakano, T. 1981, *Publ. Astron. Soc. Japan*, 33, 617
- Umebayashi, T. & Nakano, T. 1988, *Progr. Theor. Phys. Suppl.*, 96, 151

Umebayashi, T. & Nakano, T. 2009, ApJ, 690, 69

Uzdensky, D. A., & Goodman, J. 2008, ApJ, 682, 608

Wardle, M. & Königl, A. 1993, ApJ, 410, 218

Wetherill, G. W., & Stewart, G. R. 1993, Icarus, 106, 190

Zhu, Z., Hartmann, L., & Gammie, C. 2009, ApJ, 694, 1045